An Experimental Investigation of Nucleate Pool Boiling in Aqueous Solutions of a Polymer

A. D. Athavale, R. M. Manglik, and M. A. Jog
Thermal-Fluids and Thermal Processing Laboratory, College of Engineering and Applied Science, University of Cincinnati, Cincinnati, OH 45221

DOI 10.1002/aic.12616
Published online April 5, 2011 in Wiley Online Library (wileyonlinelibrary.com).

Nucleate boiling characteristics of aqueous solutions of hydroxyl ethyl cellulose (HEC QP-300; M ~ 600 kg/mol) in different concentrations ($1.0 \times 10^{-9} \leq C \leq 4.0 \times 10^{-9}$ mol/cc) are reported. These are viscous non-Newtonian, shear-thinning solutions that also display interfacial tension relaxation, which has both a concentration-dependent and temporal behavior; surface wetting increases as well, as measured by the reduction of contact angle. The measured pool boiling heat transfer from an electrically heated horizontal cylinder in $C = 1.0 \times 10^{-9}$ mol/cc aqueous solution is found to be enhanced by ~20% over the entire heat flux range ($4.0 < q''_w < 200$ kW/m^2). In higher concentration solutions, however, heat transfer degrades at low heat fluxes (incipience and partial boiling) with subsequent enhancement (~45% maximum) at high heat fluxes or in the fully-developed nucleate boiling regime. This anomalous boiling behavior in the two regimes, characterized by respectively different ebullience signatures, is shown to be scaled with changes in the liquid-solid interface wetting, vapor-liquid interfacial tension, and shear-thinning viscosity of the polymeric solutions. *AIChE J,* 58: 668–677, 2012
Keywords: heat transfer, interfacial processes, bubble phenomena, evaporation, rheology

Introduction

The ability to enhance and perhaps even control boiling, given its high heat removal efficiency, presents an exceptional thermal management opportunity for a broad spectrum of new and emerging applications.[1,2] An attractive method of altering nucleate pool boiling in water systems is to add reagents and/or polymers in controlled concentrations.[3–6] The associated heat transfer and phase-change bubble dynamics are governed by a complex interplay of interfacial behavior (vapor-liquid interfacial tension and liquid-solid surface wetting), and rheological properties of the solution. Reagents or surfactants primarily alter the surface tension and wetting of the solvent. Certain types of polymeric additives, on the other hand, besides being surface active also render the solution a non-Newtonian viscous property.

There has been growing interest in the literature in using polymers in semidilute aqueous solutions to enhance or alter nucleate boiling heat transfer, as pointed out in a recent review.[5] The reported results span a wide spectrum of phase-change characteristics, which are sometimes contradictory. For instance, Kotchaphakdee and Williams[7] found the boiling heat transfer from a plate heater to be enhanced in shear-thinning HEC-H and PA-30 solutions, of which HEC-H also reduces surface tension. Contrarily, in experiments with platinum wire heaters, Wang and Hartnett,[8] and Paul and Abdel-Khalik,[9] a deterioration in heat transfer was found in very dilute aqueous polymeric solutions when compared to that in water. To complete the quorum of dissimilar results, Yang and Maa[10] report that the boiling heat transfer

Correspondence concerning this article should be addressed to R. M. Manglik at raj.manglik@uc.edu.

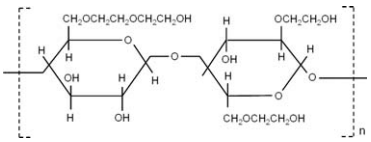

Figure 1. Schematic representation of the idealized molecular structure of the polymer hydroxyl ethyl cellulose (HEC QP-300).

performance for dilute aqueous HEC solutions is independent of heater shape (plate or platinum wire). The data of Shul'man et al.,[11] and Levitskiy et al.[12] with a plate heater and HEC-H solutions in water indicate enhanced boiling heat transfer in dilute solutions ($C = 0.015 \times 10^{-9}$ to 0.5×10^{-9} mol/cc), but decreased heat transfer in higher concentrations ($C = 10 \times 10^{-9}$ mol/cc).

The addition of some polymers in water primarily alters the solution rheology, which increases with concentration and also has a shear dependent viscous behavior.[13,14] However, depending upon their molecular chains, such polymers may also have surface-active properties, and hydroxyethyl cellulose (HEC) and polyethylene oxides are good examples.[5,15,16] In such cases, due to their molecular adsorption at the vapor-liquid and liquid-solid interface, there is some relaxation of the interfacial tension and increase in wetting of the solution,[5,17] which varies with polymer chemistry and its concentration. This significantly changes the ebullient behavior, or the bubble nucleation and departure dynamics, during boiling when compared to that in pure water.[5,12] Higher surface wetting delays incipience[18,19] but interfacial tension relaxation tends to aid smaller bubble departure and enhanced heat transfer.[4,6] The increased viscosity of the solutions, on the other hand, tends to counter this and has an adverse impact on boiling heat transfer.[5,9] The bubble growth rate and departure frequency tends to get impaired due to higher viscous drag, especially in the incipience and partial boiling regime.[5] Nevertheless, it may be hypothesized that the shear-thinning character of some polymeric solutions would tend to mitigate this effect during higher heat flux boiling of the fully-developed regime, where higher shear rates are exerted at bubble interfaces due to their substantially higher departure frequencies. This suggests a multifarious and rather complicated interrelationship, which could range from countervailing to collaborative effects of the non-Newtonian viscous behavior, surface wetting, and dynamic interfacial tension relaxation in aqueous polymeric solutions on their pool boiling heat transfer characteristics.

The objective of this study is to parametrically explore the effects of shear-dependent viscosity, along with those due to the changes in dynamic vapor-liquid interfacial tension and liquid-solid surface wettability of aqueous solutions of a surface-active polymer on their nucleate pool boiling heat transfer performance. A nonionic soluble polymer, HEC and its grade QP-300 (molecular mass ~600 kg/mol), is used as the control additive in deionized distilled water solutions. The rheological and interfacial properties of the HEC QP-300 solutions in different concentrations are recorded, which exhibit viscous shear-thinning, dynamic surface tension relaxation, and increased wetting (reduced contact angle) behaviors. Saturated pool boiling heat transfer at atmospheric pressure is measured in a controlled set of experiments with an electrically heated, horizontal cylindrical heater by mapping the variation of the applied wall heat flux q''_w with wall superheat ΔT_{sat}. The presented results characterize ebullient phase-change heat transfer from incipience or onset of nucleate boiling (ONB) to the fully developed nucleate boiling regime, and highlight the effects due to the pseudoplasticity, dynamic interfacial tension relaxation, and altered wettability of the aqueous solutions at different polymer concentrations. Furthermore, the associated bubble generation activity is photographically recorded to provide additional mechanistic insights to the vapor generation process.

Materials and Methods

Polymer solutions

The grade QP-300 of HEC, a nonionic cellulose polymer, which is used in this study, has an idealized molecular structure shown in Figure 1. It has a molecular mass of ~600 kg/mol, and it not only renders aqueous solutions with a non-Newtonian pseudoplastic (or shear thinning) rheology but also exhibits properties of a surface-active reagent (reduces surface tension). The required aqueous solutions for the experiments were prepared by adding precise quantities of HEC QP-300 powder, measured using an electronic weighing scale with ±0.1 mg accuracy, to deionized distilled water in a beaker. The homogeneity of the solution was assured by stirring it sufficiently on a magnetic stirrer so as to keep the mass moving continuously. To achieve this, ~4 hours of gentle stirring was required for complete hydration of HEC powder, and the solution was then allowed to age overnight by continuing to stir it at very slow speeds.

Pool boiling experiment

Figure 2a provides the schematic (not to scale) of the apparatus used in this study for conducting nucleate pool boiling experiments. It consists of two large corning glass vessels, where the inner glass tank, which holds the polymer solution and the cylindrical heater, is incased in the outer glass tank. Silicon oil (50 cSt), fed from a constant-temperature recirculating bath (not shown in the figure), is circulated in the outer vessel to maintain the test pool at its saturation temperature. To ensure this, the oil was maintained at a temperature (~135°C) greater than the saturation temperature of the test fluid, so as to form a thermal jacket around the pool; NESLAB's RTE-221 oil bath circulator was used for heating and circulating the silicon oil. An auxiliary electrical cartridge heater, immersed in the pool, was used to heat up the pool quickly to its saturation temperature (using the oil bath alone takes much longer time). A water-cooled reflux condenser, along with an additional coiled-tube water-cooled condenser, were used to condense the generated vapor and maintain an atmospheric-pressure, constant level pool. A U-tube manometer is mounted on top of the inner vessel, and it monitors the pool pressure with a 0.001 atm (5 mm of water column) visual accuracy throughout the pool boiling experiments.

The heating test section (described in Figure 2b) consists of a horizontal, gold plated, hollow copper cylinder of 22.2 mm outer diameter that encapsulates a 240 V, 1500 W cartridge

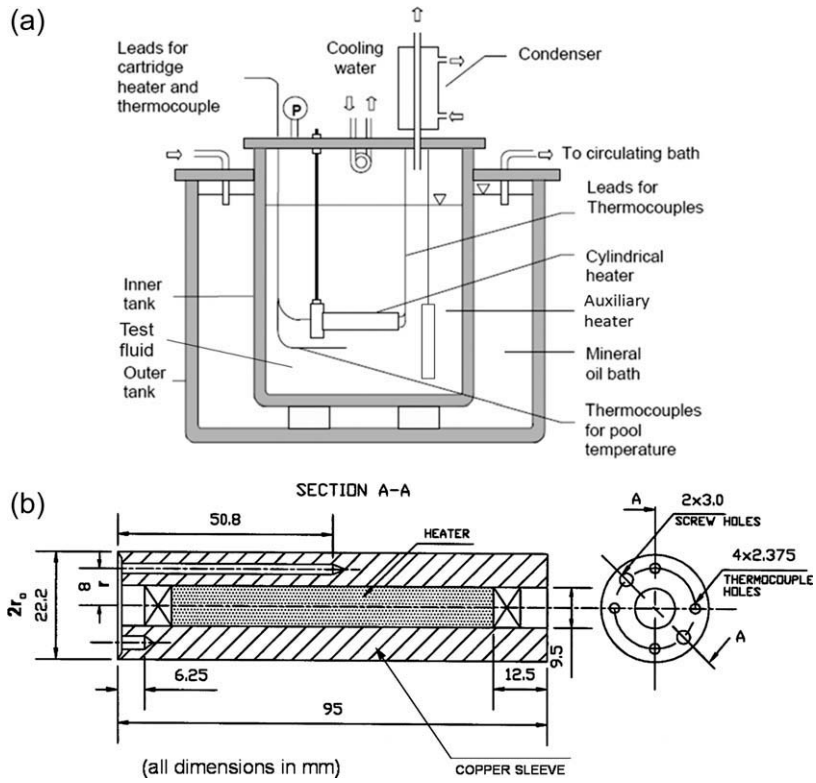

Figure 2. Experimental apparatus: (a) schematic of pool boiling set up, and (b) constructional details of cylindrical heater assembly.

heater, which has insulated and sealed (to prevent any water encroachment short-circuit) lead wires. The 0.0127-mm thick gold plating on the copper sleeve mitigates surface degradation and oxidation from the test fluids. The heater is press-fitted inside the hollow cylinder with conductive grease so as to provide good heat transfer contact with the inner walls of the outer sleeve, and the end gaps on either side are filled with silicone rubber to prevent direct water contact. Extended details of the heater test section construction and its surface characterization, which has surface roughness ranging from r.m.s. values of 0.076 to 0.347 μm, as measured by an atomic force microscope, are given elsewhere.[3,20]

The heater-wall and pool-bulk temperature measurements were made with precision ($\pm$0.5°C) copper-constantan thermocouples, connected to a computerized data acquisition system with an in-built ice junction and calibration curve. A variac-controlled AC power supply, a current shunt (0.15 Ω with 1% accuracy), and two high-precision digital multimeters for current ($\pm$2.5% accuracy) and voltage ($\pm$1.5% accuracy) were used to record the input electric power and thus determine the heat load. At each incremental value of power input or heat load, the dissipated wall heat flux q''_w was computed from the measured voltage V, current I, and heater surface area A ($= 2\pi r_o L$; where L is the length of heated heater) as,

$$q''_w = (VI/A) \tag{1}$$

In these calculations, the actual voltage drop across the heater and the actual current flowing through it (measured directly across the precision shunt resistance in series with the heater) were recorded directly to provide the actual heat load, which inherently calibrates for any temperature-dependent variations in resistance.[21,22] The wall superheat ΔT_{sat} for this heat flux was determined from the heater-wall temperature T_w, taken as the average value of four wall-temperature thermocouples reading ($T_{i,r}$) that are embedded in the heater surface, and the saturation temperature T_{sat} of the liquid pool as follows:

$$T_w = \left[\frac{1}{4}\sum_{i=1}^{4}\{T_{i,r} - (q''_w r_o/k)\ \ln(r_o/r)\}\right] \tag{2}$$

$$\Delta T_{sat} = (T_w - T_{sat}) \tag{3}$$

where r is the radius of wall thermocouple location, r_o is the cylinder heater radius, and k is the thermal conductivity of heater material. The maximum experimental uncertainties were calculated by the single-sample propagation of error method[23] were $\pm$2.92% and $\pm$0.33%, respectively, for q''_w and ΔT_{sat}.

Before the start of any experimental measurements, the pool was thoroughly degassed by first heating it to the saturation temperature by using the auxiliary heater, and then boiling it at a low heat flux while constantly maintaining it at T_{sat}. Power to the auxiliary heater was then cut off and the system was allowed to attain stable, saturation conditions; this entire process took about two-to-three hours to complete.[20] For the first set of experimental measurements, nucleate pool boiling with distilled, deionized water was recorded, with multiple runs over a period of six months so

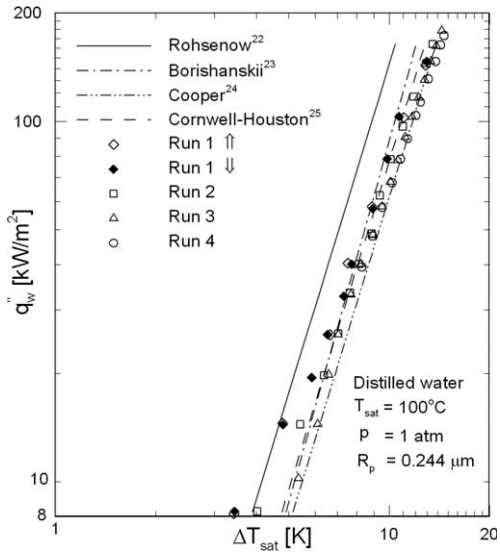

Figure 3. Nucleate pool boiling data for deionized distilled water and comparison with predictions of several correlations (Note: ⇑ and ⇓ indicates, respectively data for increasing and decreasing wall heat flux).

as to establish repeatability and the effects of aging of the heater surface. These results[20] are presented in Figure 3, where the pure water boiling data are seen to be in good agreement with some previous data,[3,4] and are also within the envelope of predictions given by the much cited Rohsenow,[24] Borishanskii,[25] Cooper,[26] and Cornwell and Houston[27] correlations. These data and the comparisons provide not only the necessary validation of measurements and data acquisition methods, but also form the essential baseline water results for evaluating and contrasting the boiling performance of aqueous polymeric solutions.

Photographic record of boiling

A PULNiX TMC-7 series high-speed CCD camera was used to capture the visual dynamics of bubble generation, growth, and motion during boiling. It has a digital resolution of 768(horizontal) × 494(vertical) pixels, with eight different shutter speeds that go up to 1/10,000 sec. The camera is also fitted with FUJI 12.5 mm × 75 mm zoom lens for capturing close-up photographs during different stages of boiling. The camera was interfaced with a PC using a USB-based digital image capture and processing system (DQP-A4 Premier), which records consecutive frames of video in real-time images at 60 frames/s.

Viscosity measurement

Viscosity measurements were made using a rotating cup-and-cylinder rheometer (AR-2000, TA Instruments) and a set of five Cannon-Fenske capillary-tube viscometers of different capillary diameters. The test solution were prepared by carefully adding a precisely weighed (±0.1 mg accuracy on an electronic scale) quantity of polymer powder to deionized distilled water. The mixture was then stirred at a constant speed on a magnetic stirrer till the powder dissolved completely, and the solution was then aged over a period of 10-12 hours before making viscosity measurement. Using the concentric cylinder assembly in the AR-2000 rheometer, apparent viscosity data in the shear-rates range of 10 s^{-1} to 400 s^{-1} were obtained, where the temperature control was maintained by the built-in Peltier heating system in the rheometer. The higher shear rate data were obtained from the set of capillary-tube viscometers; note that the shear rate in these instruments is a function of their respective capillary diameters. Furthermore, a capillary-tube viscometer was also used for the measurements with weak concentration aqueous solutions so as to obtain the intrinsic viscosity, or the limiting viscosity number of the polymer.[17,28,29] Once again, the maximum single-sample error propagation method based uncertainty[23] in viscosity and temperature were ±1.4% and ±0.5%, respectively.

Surface tension measurement

Both the equilibrium and dynamic surface tension, or the gas-liquid interfacial tension, measurements of the polymer solutions were made using a tensiometer (SensaDyne QC6000; Chem-Dyne Research Corp.) that operates on the maximum bubble pressure method. It has two glass capillary-tube orifices of unequal diameters that are immersed in the test fluid pool in a beaker. The test fluid is maintained at a constant temperature, which is measured using a well-calibrated thermistor (±0.1°C precision) attached to the orifice probes. When dry air is bubbled through the orifices, a differential pressure signal is produced, which is proportional to the gas-liquid interfacial tension. Also, the time interval between the newly formed interface and the point of bubble break-off at the orifice mouth is referred to as the surface age τ of interface. It gives the measurement of bubble growth time that corresponds to the dynamic surface tension value at a given operating bubble frequency. Thus, by altering the air-bubble frequencies through the probes, both equilibrium and dynamic surface tension can be measured; the equilibrium data are obtained with very low bubble frequencies that lead to static or unchanging conditions. Details of the calibration and measurement validation procedures are given in.[15] The maximum uncertainties[23] in solution concentration, temperature, and surface tension measurements were found to be ±0.4%, ±0.5%, and ±0.7%, respectively.

Contact angle measurement

The static contact angle was measured with a sessile-drop goniometer. A small drop of the test solution was carefully deposited on a stainless steel specimen substrate that was placed under the goniometer lens. A precision microsyringe was used to produce a droplet of desired liquid volume (~2 to 3 μl; drop volume ≤ volume of a spherical drop with a radius equal to the capillary length[*] l_c), which was carefully placed on the specimen substrate. The contact angle was measured for several new droplets placed at different surface

[*] This is the characteristic length scale for a liquid droplet that represents the balance between gravitational and surface tension forces. Thus, a sessile drop volume with an equivalent spherical radius less than l_c would have negligible influence of its weight and its spread on any substrate would be dominated by surface tension and consequent wetting alone.

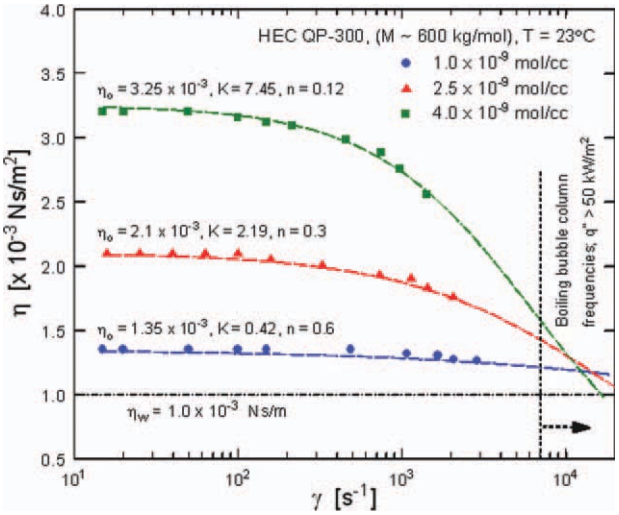

Figure 4. Shear-rate dependent apparent viscosity variation for different concentrations of aqueous HEC QP-300 solutions.

[Color figure can be viewed in the online issue, which is available at wileyonlinelibrary.com.]

locations on the substrate after allowing a one-minute settling time in each case. The goniometer radius line was aligned tangentially to the edge of the droplet touching the substrate specimen, and the contact angle was then directly measured from the angular scale engraved on the eyepiece. The minimum precision in this measurement was $\pm 0.5^{\circ}$.

Results and Discussion

Aqueous solutions of HEC QP-300, except in low concentrations, generally display a viscous pseudoplastic behavior. This non-Newtonian characteristic is pointed out by Figure 4, where the variations in shear-rate dependent apparent viscosity (η = shear stress / shear rate) are graphed for HEC QP-300 solutions in there different concentrations. At low shear rates the solution rheology tends to be Newtonian, with a significantly higher viscosity than the solvent, and the shear-thinning non-Newtonian flow manifests only at high shear rates. The consequent apparent viscosity behavior can be represented by the modified cross model.[30–32] This constitutive relationship, for the case of a negligible infinite shear-rate asymptote, in essence, is functionally the same as the modified power-law model,[33] and can be expressed as

$$\eta = \eta_o \left[1 + (\eta_o/K)\gamma^{1-n}\right]^{-1} \tag{4}$$

For the rheology of three HEC QP-300 solutions graphed in Figure 4, the range of the characteristic parameters are $1.35 \times 10^{-3} \leq \eta_o$ [N s/m^2] $\leq 3.25 \times 10^{-3}$, $0.42 \leq K$ [N s^n/m^2] ≤ 7.45, and $0.12 \leq n \leq 0.6$. The low values of flow-behavior index n are indicative of the highly shear-thinning or pseudoplastic property of these solutions.

A more fundamental measure of the ability of a polymer to alter the solvent viscosity in solution, is the intrinsic viscosity $[\eta]$ of the polymer.[29,34] Also referred to as the limiting viscosity number, and as Staudinger's index in older literature,[35] the intrinsic viscosity $[\eta]$ for HEC QP-300 was determined by measuring the viscosity η with several different weak-concentration aqueous solutions using a capillary viscometer. From these measurements and knowing the solvent viscosity η_s (water in this case), the specific viscosity η_{sp} and relative viscosity η_{rel}, respectively, for each dilute concentration solution can be determined as follows:

$$\eta_{sp} = [(\eta - \eta_s)/\eta_s], \quad \text{and} \quad \eta_{rel} = (\eta/\eta_s)$$

Thus, by extrapolating the graph of (η_{sp}/C) vs. C to zero concentration, the intercept of the consequent Huggins plot gives the value for $[\eta]$; this can also be obtained from the intercept of the Kraemer plot through the graph of $\ln[\eta_{rel}/C]$ vs. C. The two plots are given in Figure 5, and the average value of $[\eta]$ for HEC QP-300 was determined to be 5.29 dl/g. This limiting value at infinite dilution is a direct measure of the molecular properties of the polymer, and it essentially quantifies the volume occupied by a unit mass of the macromolecule. Higher $[\eta]$ suggests increased capability of a polymer to enhance the solution viscosity, and in general it is related to the molecular weight or degree of polymerization.[28,36,37]

The variation in equilibrium surface tension, or the liquid-vapor interfacial tension, with different bulk concentrations of the polymer HEC QP-300 in water is graphed in Figure 6. The surface tension is seen to continually decrease from that of the solvent (water; $\sigma_w = 72.4 \times 10^{-3}$ N/m) to a minimum asymptotic value of 66.8×10^{-3} N/m. The concentration that demarcates the lower inflection point in the $\sigma - C$ isotherm, i.e., the point of transition to the minimum surface tension asymptote, often coincides with the critical polymer concentration (cpc) or overlap concentration C^*.[5,36,38,39] At cpc or C^*, polymer agglomeration or coil entanglements begin to form in solution, which would then be in the semi-dilute regime. This interfacial tension relaxation is a diffusion-rate dependent behavior, which is generally governed by the bulk concentration and diffusion-adsorption kinetics of the polymer-solvent systems.[40] The critical polymer concentration, as discerned from Figure 6, is estimated to be $\sim 1.0 \times 10^{-9}$ mol/cc ($\sim$600 wppm).

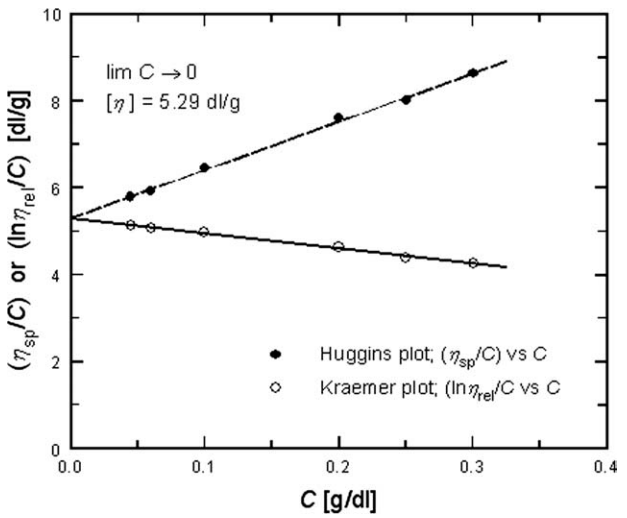

Figure 5. Intrinsic viscosity $[\eta]$ of HEC QP-300.

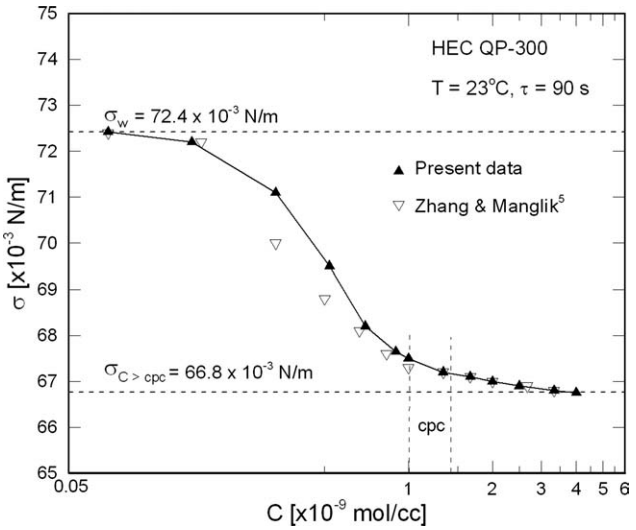

Figure 6. Equilibrium gas-liquid interfacial tension (surface tension) and its variation with polymer concentration in aqueous solution.

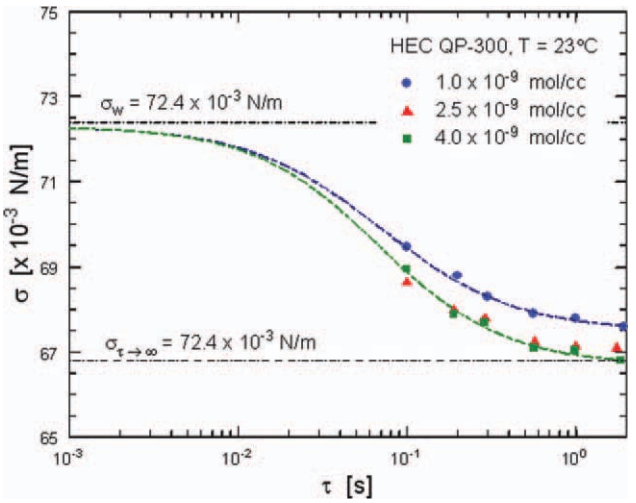

Figure 7. Temporal variation of dynamic surface (gas-liquid interfacial) tension for different polymer concentration aqueous solutions.

[Color figure can be viewed in the online issue, which is available at wileyonlinelibrary.com.]

The critical overlap concentration can also be determined from the intrinsic viscosity,[28,34,36,37] because $[\eta]^{-1}$ approximately represents the concentration within the polymer, or its overlap concentration in a solvent, exceeding which molecules will touch and interpenetrate to form a semidilute solution. According to the Einstein model, which considers dilute dispersions of unsolvated spherical particles, when the volume fraction ϕ of the spherical particles is small the relative viscosity is given by the following function[34]:

$$\frac{\eta}{\eta_s} = 1 + 2.5\phi + k_1\phi^2 + \ldots \quad (5)$$

From the limiting condition of Eq. 5 it can be shown[34,37] that as $\phi \rightarrow 0$ the overlap concentration can be approximated as $C^* \approx 0.25[\eta]^{-1}$. Thus, from the intrinsic viscosity given by the plots in Figure 5, the critical polymer concentration is obtained as $C^* \approx 0.79 \times 10^{-9}$ mol/cc. This value is the same order of magnitude as that obtained from the gas-liquid interfacial tension adsorption isotherm of Figure 6, and corroborates the latter results.

Furthermore, that the liquid-vapor interfacial tension relaxation is a time-dependent process is demonstrated by the σ vs. τ plots of Figure 7. Here, the change in surface tension σ with surface age τ, or the time period of a newly formed bubble from inception to departure, is graphed for aqueous solutions of HEC QP-300 with bulk concentrations of $1.0 \times 10^{-9} \leq C \leq 4.0 \times 10^{-9}$ mol/cc. It is seen that a finite time is required for complete interface relaxation, or to attain an equilibrium between the surface and bulk concentrations. Generally a surface age of $\tau > 1.0$ s is needed for this condition, and for $\tau < 50$ ms, the interfacial tension essentially corresponds to that of the solvent (water); the interim period of 50 ms $< \tau <$ 1.0 s is characterized by sharp gradients in σ. It may be noted here that the values for σ at very small surface age are extrapolated from the time-dependent adsorption isotherm fit through the data by the method outlined by Hua and Rosen.[41] Also, there is little difference between the data for 2.5×10^{-9} and 4.0×10^{-9} mol/cc solutions, suggesting micelle agglomeration or coil entanglements of the polymer at these concentrations. This dynamic surface tension behavior, which is facilitated and governed by the molecular mobility of the polymer in solution and its interfacial adsorption[15,40–42] at an evolving gas-liquid interface, lends to the modification of ebullience that characterizes the attendant boiling heat transfer.

The change in wetting, manifest at a liquid-solid interface, can be ascertained by the contact angle θ, and its variation with concentration C of HEC QP-300 in aqueous solutions is graphed in Figure 8. The measurement is for a metallic substrate (stainless steel), and θ is seen to decrease with increasing C till a lower constant-value asymptote is attained. The

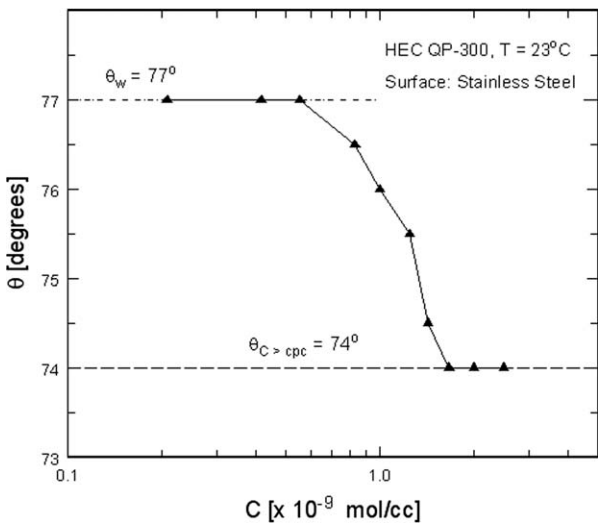

Figure 8. Change in contact angle with concentration of aqueous HEC QP-300 solutions.

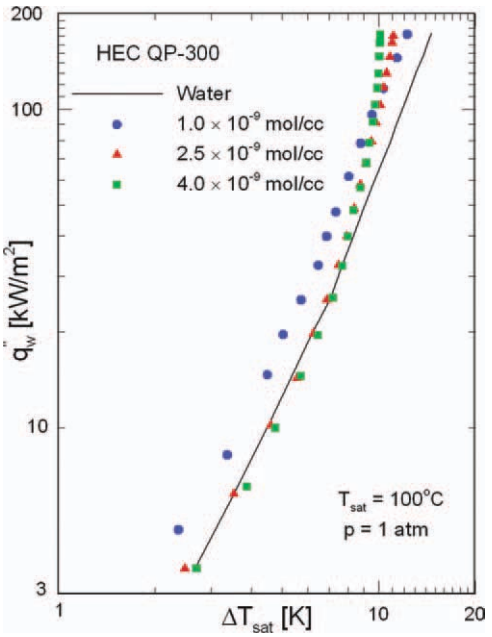

Figure 9. Nucleate pool boiling data for different concentrations of aqueous HEC QP-300 solutions, along with that for distilled, deionized water.

[Color figure can be viewed in the online issue, which is available at wileyonlinelibrary.com.]

minimum contact angle plateau is further seen to be attained when $C > C^*$ (the overlap concentration), where molecular agglomeration of the polymer begins to form in solution. This is representative of typical physisorption behavior of surface-active solutes at liquid-solid interfaces, and where wetting is influenced by the kinetics of interfacial molecular adsorption.[43,44]

In general, the boiling behavior of a liquid is altered by the changes in its surface tension, rheology, and heater surface wettability. While wetting of the heater surface controls nucleation and the site density thereof, gas-liquid interfacial tension and shear-dependent viscosity of a polymeric solution alters the postnucleated bubble dynamics.[4–6] The pool boiling curves presented in Figure 9 for different concentrations of aqueous HEC QP-300 solutions, along with that for distilled and deionized water, quantify this ebullient heat transfer behavior. The substantial leftward shift in the $q''_w \sim \Delta T_{sat}$ curve for $C = 1.0 \times 10^{-9}$ mol/cc ($\sim C^*$ or cpc) relative to that for water is indicative of the heat transfer enhancement over the entire range of heat flux considered in the experiments. This specific case represents the largest overall enhancement, which is consistent with the previous finding that the highest boiling performance is attained with critical or overlap concentration of the polymer.[5] However, an anomalous boiling behavior is seen in solutions with higher concentration ($C = 2.5 \times 10^{-9}$ and 4.0×10^{-9} mol/cc). There is a significant rightward shift in the boiling curve where the heat transfer is even less than that in water in the low-heat-flux partial-boiling regime, followed by much larger enhancement, relative to that with C^*, at higher hear fluxes (>100 kW/m^2) or the fully-developed boiling regime.

A much clearer and quantitatively amplified delineation of the boiling performance of the three different concentration solutions of HEC QP-300, relative to that in distilled water, is presented in Figure 10. The variation of the enhanced heat transfer coefficient, quantified by the dimensionless ratio $[(h - h_w)/h_w]$ with the heater-wall heat flux q''_w is graphed. The consistent and virtually constant enhancement of about 20% in the 1.0×10^{-9} mol/cc ($\sim C^*$) HEC concentration aqueous solution is evident in Figure 10, along with the agreement with previous data.[5] As indicated earlier, the more curiously unexpected set of results are those for solutions with $C = 2.5 \times 10^{-9}$ and 4.0×10^{-9} mol/cc. In these cases, there is a reduction (or degradation with respect to pure water) in heat transfer when $q''_w < 30$ kW/m^2, but much larger enhancement than that with C^* when $q''_w > 100$ kW/m^2. The higher of the two concentrations lends to about 6% decrease in heat transfer when compared with water for $7 < q''_w < 30$ kW/m^2. This is a direct consequence of the higher polymeric solution viscosity (2-to-3× water, as seen in Figure 4) at low shear rates and the consequent drag effects at the liquid-vapor interface of ebullient transport in the partial boiling regime. With increasing heat flux and hence larger vapor generation, the interfacial shear rate increases and thereby the viscosity of the shear-thinning solutions decreases; at very high shear rates the higher concentration solution even becomes less viscous than the lower C ones (see Figure 4). As a result, the retarding viscous forces at the bubble-liquid pool interface become less significant and the low-surface-tension-driven enhancement, characterized by smaller and higher frequency bubble generation, is re-established with peak heat transfer performance attained when $q''_w > 100$ kW/m^2.

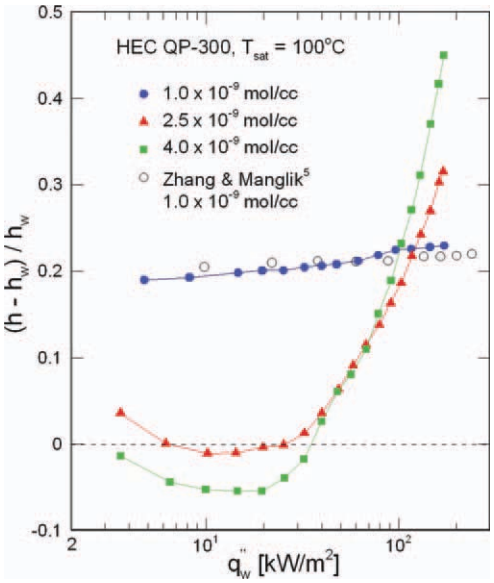

Figure 10. Variation of enhancement in boiling heat transfer coefficient with wall heat flux in different concentrations of aqueous HEC QP-300 solutions.

[Color figure can be viewed in the online issue, which is available at wileyonlinelibrary.com.]

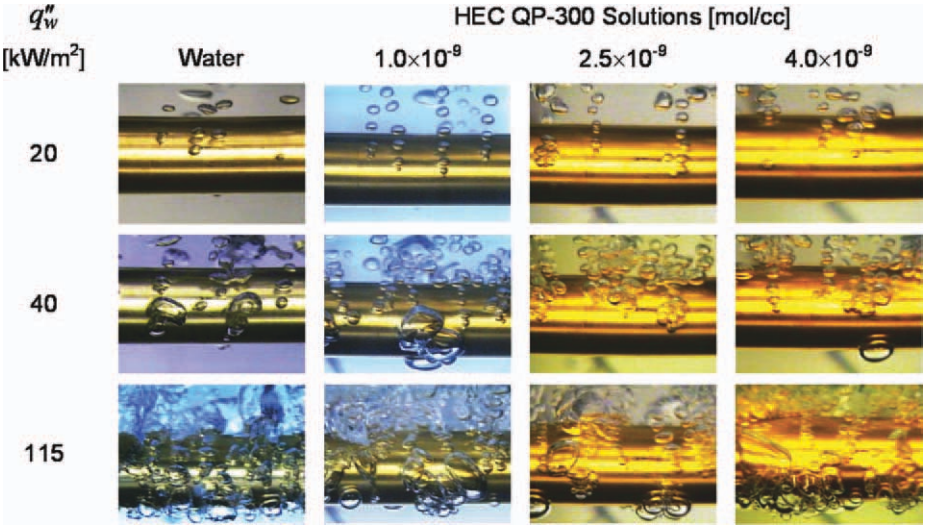

Figure 11. Ebullient or bubbling behavior during boiling of pure water and aqueous solutions of HEC QP-300 in different molar concentrations.

[Color figure can be viewed in the online issue, which is available at wileyonlinelibrary.com.]

The nucleate boiling performance can further be characterized by the respective ebullient signatures in the three solutions at different heat fluxes. Photographic records of the vapor production that characterize the boiling history for increasing heat flux (q''_w = 20, 40 and 115 kW/m^2) are presented in Figure 11. The bubble generation features, described by their relative shape, size, coalescence activity, and surface density and distribution in the polymer solutions are seen to be very distinct from that in water. The boiling is more vigorous in $C \sim C^*$ ($= 1.0 \times 10^{-9}$ mol/cc) solutions, which is distinguished by smaller bubble production, spread over a wider portion of the heater surface with the entire range of heat fluxes considered in the experiments. There is reduced coalescence of bubbles that have a higher departure frequency, both outcomes of reduced liquid-vapor interfacial tension. Also, molecular physisorption of the polymer on the heater surface may contribute to the formation of new sites,[5,11,12] which would perhaps account for the increase in number of nucleation sites despite a slight increase in the surface wettability (as indicated by the small reduction in contact angle shown in Figure 8).

However, in the larger concentration solutions ($C > C^*$, or $C = 2.5 \times 10^{-9}$ and 4.0×10^{-9} mol/cc) and at low heat fluxes ($q''_w = 20$ kW/m^2, or the partial boiling regime), the extent of bubbling activity decreases substantially (Figure 11). This is possibly due to the increased viscosity of the higher concentration polymer solution, as seen in Figure 4, where the zero-shear rate viscosity η_o increases as $1.35 \times 10^{-3} \rightarrow 2.1 \times 10^{-3} \rightarrow 3.2 \times 10^{-3}$ N s/m^2 or about $\sim$1.6$\times$ to 2.4$\times$ that at C^*. The consequent higher viscous drag at the dynamic vapor-liquid interface tends to suppress or retard the postnucleation growth of vapor bubbles. This then leads to increasing deterioration of boiling performance with polymer concentration C at lower heat fluxes. The relatively higher shear rate associated with greater vapor generation when $q''_w \geq 40$ kW/m^2, on the other hand, lowers the viscosity of the shear-thinning or pseudoplastic solutions. With the attendant reduction in viscous retardation at the vapor-liquid interface re-establishes the dominance of interfacial tension relaxation of higher concentration polymeric solution, and the bubbling activity again increases. The shear thinning behavior is more pronounced in the $C = 4.0 \times 10^{-9}$ mol/cc solution, thereby further intensifying the ebullience and the boiling heat transfer.

Conclusions

That different bulk concentrations of the polymer additive HEC QP-300 in water anomalously alter the nucleate boiling heat transfer performance is evident from the results presented in Figures 9–11. The primary controlling influence is rendered by the rheology of the solution, which ranges from a highly viscous behavior to shear-thinning characteristics with increasing shear rates. Both the viscous nature and pseudoplasticity in turn increase with the polymer concentration, and this diversely affects the different boiling regimes; in the partial boiling, low-frequency bubble-generation regime the viscous behavior dominate, whereas in the fully developed, high-frequency bubble-generation regime the shear-thinning behavior of the polymeric solution has greater influence. Furthermore, the reduction in dynamic surface tension (which alters the required superheat for the onset of boiling and postdeparture bubble frequency), and possibly the macromolecular physisorption of the polymer onto the heating surface (which perhaps aids the formation of new nucleation sites) are also the controlling factors for the boiling heat transfer enhancement in lower the concentration ($C \sim C^*$) solution.

Improvements in the boiling performance, varying from 19 to 22% increase in the heat transfer coefficient relative to that in pure water, were obtained with $C = 1.0 \times 10^{-9}$ mol/cc over the entire heat flux range of the experiments. On the other hand, the reduction in nucleate boiling heat transfer coefficients with higher concentrations ($C > C^*$) at low heat flux levels is caused by the retardation of vapor-bubble growth and postdeparture bubble frequency, possibly due to

the viscous suppression of microconvection in the bubble boundary layer. This decreased ebullience, observed in the partial boiling regime, is reversed and augmented at higher heat fluxes ($q''_w > 40$ kW/m^2) where the higher shear rate at vapor-liquid interfaces of bubble that are more vigorously produced lends to a shear-thinning viscous behavior in the solution. The enhancement in the fully developed boiling regime produces a peak performance when $q''_w > 100$ kW/m^2, and up to 45% increase in the boiling heat transfer coefficient, compared to that in pure water, is obtained with $C = 4.0 \times 10^{-9}$ mol/cc.

Notation

A = cylindrical heater surface area, $2\pi r_o L$ (m^2)
C = concentration (mol/cc)
C^* = critical polymer concentration or overlap concentration (mol/cc)
g = gravitational acceleration (m/s^2)
h = heat transfer coefficient (W/m^2 K)
h_w = heat transfer coefficient of water (W/m^2 K)
I = current (A)
K = consistency index, Eq. 4 (N s^n/m^2)
k_1 = constant in Einstein's viscosity model, Eq. 5 (-)
L = heated length of cylindrical heater (m)
l_c = capillary length, $\sqrt{\sigma/\rho g}$ (m)
M = molecular weight (kg/mol)
n = flow behavior index, Eq. 4 (-)
p = pressure, (N/m^2)
q''_w = heat flux (kW/m^2)
R_p = average surface roughness of heater, Figure 3, (μm)
r = radius of embedded thermocouple location in cylindrical heater, Eq. 2 (m)
r_o = outer radius of cylindrical heater surface (m)
T_w = temperature of heater surface (K)
T_{sat} = saturation temperature of test liquid pool (K)
ΔT_{sat} = wall superheat or wall-to-pool temperature difference, ($T_w - T_{sat}$) (K)
V = voltage (V)
ϕ = volume fraction of spherical particles in dilute dispersions (-)
γ = shear rate (s^{-1})
η = viscosity and/or apparent viscosity of polymeric solution (N s/m^2)
$[\eta]$ = intrinsic viscosity (dl/g)
η_o = zero shear-rate viscosity of polymeric solution (N s/m^2)
η_{rel} = relative viscosity, (η/η_s) (-)
η_s = viscosity of solvent (N s/m^2)
η_{sp} = specific viscosity, ($\eta - \eta_s$)/η_s (-)
ρ = liquid density (kg/m^3)
σ = surface tension (N/m)
τ = surface age of bubble (s)

Acknowledgments

This work was supported by the National Science Foundation (grant no. CBET-0755720) and by the US Department of Energy (NEER grant no. DE-FG07-07ID14772). Also, the facilities provided by the Thermal-Fluids & Thermal Processing Laboratory, and the experimental support work of Rupesh Bhatia, Rohit Gupta, and Vishaul Ravi are gratefully acknowledged.

Literature Cited

1. Bergles AE. *New frontiers in enhanced heat transfer*. In: Manglik RM, Ravigururajan TS, Muley A, Papar RA, Kim J, editors. *Advances in Enhanced Heat Transfer*. Vol HTD-Vol. 365. New York, NY: ASME, 2000:1–8.
2. Manglik RM. *Heat transfer enhancement*. In: Bejan A, Kraus AD, editors. *Heat Transfer Handbook*. New York, NY: Wiley, 2003.
3. Wasekar VM, Manglik RM. Pool boiling heat transfer in aqueous solutions of an anionic surfactant. *J Heat Transfer*. 2000;122:708–715.
4. Zhang J, Manglik RM. Additive adsorption and interfacial characteristics of nucleate pool boiling in aqueous surfactant solutions. *J Heat Transfer*. 2005;127:684–691.
5. Zhang J, Manglik RM. Nucleate pool boiling of aqueous polymer solutions on a cylindrical heater. *J Non-Newtonian Fluid Mech*. 2005;125:185–196.
6. Manglik RM, Jog MA. Molecular-to-large-scale heat transfer with multiphase interfaces: current status and new directions. *J Heat Transfer*. 2009;131:121001.
7. Kotchaphakdee P, Williams MC. Enhancement of nucleate pool boiling with polymeric additives. *Int J Heat Mass Trans*. 1970; 13:835–848.
8. Wang ATA, Hartnett JP. Influence of surfactants on pool boiling of aqueous polyacrylamide solutions. *Wärme-und Stoffübertragung*. 1992;27:245–248.
9. Paul DD, Abdel-Khalik SI. Saturated nucleate pool boiling bubble dynamics in aqueous drag-reducing polymer solutions. *Int J Heat Mass Trans*. 1984;27:2426–2428.
10. Yang YM, Maa JR. Effects of polymer additives on pool boiling phenomena. *Lett Heat Mass Trans*. 1982;9:237–244.
11. Shul'man ZP, Khusid BM, Levitskiy SP. Special features of boiling of macromolecular polymer solutions. *Heat Trans Res*. 1993; 25:872–878.
12. Levitskiy SP, Khusid BM, and Shul'man ZP. Growth of vapor bubbles in boiling polymer solutions-II. Nucleate boiling heat transfer. *Int J Heat Mass Trans*. 1996;39:639–644.
13. Carreau PJ, De Kee DCR., Chhabra RP. *Rheology of Polymeric Systems: Principles and Applications*. New York, NY: Hanser Gardner Publications, 1997.
14. Chhabra RP, Richardson JF. *Non-Newtonian Flow in the Process Industries: Fundamentals and Engineering Applications*. Oxford, UK: Butterworth-Heinemann, 1999.
15. Manglik RM, Wasekar VM, Zhang J. Dynamic and equilibrium surface tension of aqueous surfactant and polymeric solutions. *Exp Therm Fluid Sci*. 2001;25:55–64.
16. Hu RYZ, Wang ATA, Hartnett JP. Surface tension measurement of aqueous polymer solutions. *Exp Therm Fluid Sci*. 1991;4:723–729.
17. Holmberg K, Jönsson B, Kronberg B, Lindman B. *Surfactants and Polymers in Aqueous Solution*, 2nd ed. New York, NY: Wiley, 2003.
18. Bergles AE. *Fundamentals of boiling and evaporation*. In: Kakaç S, Bergles AE, Fernandes EO, editors. *Two-Phase Flow Heat Exchangers: Thermal-Hydraulic Fundamentals and Design*. The Netherlands: Kluwer, 1988:159–200.
19. Kenning DBR. What do we really know about nucleate boiling. Presented at the IMechE Transactions, 6th UK National Heat Transfer Conference. Edinburgh, UK: Bury St. Edmunds, September 15-16, 1999:143–167.
20. Athavale AD. *Characterization of nucleate pool boiling heat transfer of aqueous polymeric solutions [M.S.]*. Cincinnati, OH: Mechanical Engineering, University of Cincinnati, 2011.
21. Jung C, Bergles AE. Evaluation of commercial enhanced tubes in pool boiling. Troy, NY: Rensselaer Polytechnic Institute, 1989. Technical Report No. DE-FC07–88ID.
22. Wasekar VM, Manglik RM. Nucleate pool boiling heat transfer in aqueous surfactant solutions. Cincinnati, OH: University of Cincinnati, 2001. Technical Report No. TFTPL-4.
23. Moffatt RJ. Describing the uncertainties in experimental results. *Exp Therm Fluid Sci*. 1988;1:3–17.
24. Rohsenow WM. A Method of correlating heat transfer data for surface boiling of liquids. *Trans ASME*. 1952;74:969–976.
25. Borishanskii VM. *Correlation of the effect of pressure on the critical heat flux and heat transfer rates using the theory of thermodynamic similarity*. In: Kutateladze SS, editor. *Problems of Heat Transfer and Hydraulics of Two-Phase Media*. New York, NY: Pergamon Press, 1969:16–37.
26. Cooper MG. Saturated nucleate pool boiling—a simple correlation. Presented at the First U.K. National Conference on Heat Transfer. University of Leeds, UK, July 3-5, 1984.
27. Cornwell K, Houston SD. Nucleate pool boiling on horizontal tubes: a convection-based correlation. *Int J Heat Mass Trans*. 1994;37 (Suppl 1):303–309.
28. Hiemenz PC. *Polymer Chemistry: The Basic Concepts*. New York, NY: Marcel Dekker, 1984.

29. Macosko CW. *Rheology: Principles, Measurements, and Applications*. New York, NY: Wiley, 1994.
30. Cross MM. Rheology of non-Newtonian fluids: a new flow equation for pseudoplastic systems. *J Colloid Sci*. 1965;20:417–437.
31. Soong D, Shen M. Shear-rate-dependent viscosity of non-Newtonian suspensions and entangled polymer systems. *Polym Eng Sci*. 1980;20:1177–1180.
32. Castelain C, Doublier JL, Lefebvre J. A study of the viscosity of cellulose derivatives in aqueous solutions. *Carbohydr Polym*. 1987;7:1–16.
33. Dunleavy JE, Middleman S. Correlation of shear behavior of solutions of polyisobutylene. *J Rheol*. 1966;10:157–168.
34. Hiemenz PC, Rajagopalan R. *Principles of Colloid and Surface Chemistry*, 3rd ed. New York, NY: Marcel Dekker, 1997.
35. Ibrahim FW. Correct determination of staudinger's index (intrinsic viscosity) and of huggins constant. *J Polym Sci Part A: Gen Pap*. 1965;3:469–478.
36. De Gennes P. *Scaling Concepts in Polymer Physics*. Ithaca, NY: Cornell University Press, 1979.
37. Foroutan M, Khoee S, Zarrabi M. Overlap concentration of an aqueous poly(N-vinylcaprolactam) solution in the dynamic and static states. *J Appl Polym Sci*. 2008;109:597–601.
38. Broseta D, Leibler L, Lapp A, Strazielle C. Universal properties of semi-dilute polymer solutions: a comparison between experiments and theory. *Europhys Lett*. 1986;2:733–737.
39. Cosgrove T, Griffiths PC. The critical overlap concentration measured by pulsed field gradient nuclear magnetic resonance technique. *Polymer*. 1994;35:509–513.
40. Miller CA, Neogi P. *Interfacial Phenomena: Equilibrium and Dynamic Effects*. New York, NY: Marcel Dekker, 1985.
41. Hua XY, Rosen MJ. Dynamic surface tension of aqueous surfactant solutions. I. Basic parameters. *J Colloid Interface Sci*. 1988; 124:652–659.
42. Miller R, Joos P, Fainerman VB. Dynamic surface and interfacial tensions of surfactant and polymer solutions. *Adv Colloid Interface Sci*. 1994;49:249–302.
43. Kwok DY, Neumann AW. Contact angle measurement and contact angle interpretation. *Adv Colloid Interface Sci*. 1999;81:167–249.
44. Lee KS, Ivanova N, Starov VM, Hilal N, Dutschk V. Kinetics of wetting and spreading by aqueous surfactant solutions. *Adv Colloid Interface Sci*. 2008;144:54–65.

Manuscript received Dec. 17, 2010, and revision received Feb. 8, 2011.